INTERNATIONAL JOURNAL FOR NUMERICAL METHODS IN FLUIDS, VOL. 17, 787–801 (1993)

INTEGRAL TRANSFORM ANALYSIS OF NATURAL CONVECTION IN POROUS ENCLOSURES

CAI BAOHUA AND R. M. COTTA

Programa de Engenharia Mecânica-EE/COPPE/UFRJ, Universidade Federal do Rio de Janeiro, Cx. Postal 68503- Cidade Universitária, Rio de Janeiro-RJ 21945, Brazil

SUMMARY

A hybrid numerical-analytical solution for steady-state natural convection in a porous cavity is proposed, based on application of the ideas in the generalized integral transform technique. The integral transformation process reduces the original coupled partial differential equations, for temperature and stream function, into an infinite system of non-linear ordinary differential equations for the transformed potentials, which is adaptively truncated and numerically solved through well-established algorithms. The approach is applied to a vertical rectangular enclosure subjected to uniform internal heat generation. The convergence characteristics of the explicit inversion formulae are illustrated and critical comparisons with previously reported purely numerical solutions are performed.

KEY WORDS Integral Transforms Natural Convection Porous Media Numerical Methods

INTRODUCTION

Natural convection phenomena in porous media represent one important segment of the heat and mass transfer field, with direct applications in thermal insulations, radioactive waste disposal, solar energy collectors and geothermal energy analysis. Various contributions appeared in the literature within the last two decades, which are reviewed in References 1–4. More specifically, natural convection within two-dimensional porous enclosures has been dealt with computationally through well-known finite difference[1–3] and finite element techniques,[4] besides approximate asymptotic solutions.[1] In addition to the interesting physics pertinent to this class of problems, the associated system of coupled elliptic partial differential equations for temperature and stream function, provides an important test case in the development of new solution techniques for convection–diffusion problems.

Within the last few years, the ideas in the so-called generalized integral transform technique,[5] were progressively advanced towards the establishment of an alternative hybrid numerical–analytical approach, for *a priori* non-transformable diffusion and convection–diffusion problems. Based on the formal analytical principles in the classical integral transformation method,[6] various classes of linear problems, not *a priori* tractable through this classical method, were handled. Such developments are systematically presented in Reference 5 and include situations of variable equation and boundary coefficients, irregular geometries, unseparable eigenvalue problems, moving boundaries and conjugated and coupled problems, etc. More recently, the same basic principles were successfully employed in the analysis of non-linear diffusion[7,8] and convection–diffusion problems.[9–12] The present note is, therefore, one more step

0271–2091/93/210787–15$12.50
© 1993 by John Wiley & Sons, Ltd.
Received January 1992
Revised May 1993

in the effort of reaching the full potential of this promising approach, by testing its performance in the class of problems represented by steady-state natural convection within a two-dimensional porous cavity. The technique is illustrated by considering a vertical rectangular porous enclosure, subjected to uniform internal heat generation and cooling from the side walls. This example was thoroughly studied in Reference 1 through a careful implementation of the control volume approach,[13] providing extensive results for validation purposes.

The proposed integral transformation eliminates the dependence on one of the co-ordinates and yields a denumerable system of second-order non-linear Ordinary Differential Equations (ODE) for the transformed temperature and stream function. This ODE system is then truncated to a sufficiently large finite order and numerically solved through well-established algorithms for boundary value problems, available in scientific subroutines libraries[14] with appropriate automatic error control. The explicit inversion formula then recovers the original potentials, providing an analytical solution in the transformed direction. The convergence behaviour of the inversion formula is demonstrated here for a few representative values of the governing parameters, Rayleigh number and aspect ratio. Also, fully converged results for temperature and Darcy velocities are used to validate the previously reported purely numerical solutions.

ANALYSIS

We consider two-dimensional, steady natural convection in a saturated porous rectangular enclosure, subjected to an uniform internal heat generation and to cooling at both side walls, which are kept at the same uniform temperature. The top and bottom ends are kept insulated, according to Figure 1. Within the validity of Darcy's law and after invoking the Boussinesq approximation, the problem formulation in dimensionless form is given by[1]

$$\frac{\partial^2\psi(x,y)}{\partial y^2}+\frac{\partial^2\psi(x,y)}{\partial x^2}=-Ra\frac{\partial T(x,y)}{\partial x}, \tag{1a}$$

$$\frac{\partial^2 T}{\partial y^2}+\frac{\partial^2 T}{\partial x^2}+1=\frac{\partial\psi}{\partial y}\frac{\partial T}{\partial x}-\frac{\partial\psi}{\partial x}\frac{\partial T}{\partial y}, \quad \text{in } 0<x<1,\ 0<y<A, \tag{1b}$$

with boundary conditions

$$\psi(0,y)=\psi(1,y)=0, \qquad T(0,y)=T(1,y)=0, \tag{1c–f}$$

$$\psi(x,0)=\psi(x,A)=0, \qquad \frac{\partial T(x,0)}{\partial y}=\frac{\partial T(x,A)}{\partial y}=0, \tag{1g–j}$$

where various dimensionless groups are defined as[1]

$$x=\frac{x^*}{d}, \qquad y=\frac{y^*}{d}, \qquad \psi=\frac{\psi^*}{\alpha}, \qquad A=\frac{h}{d},$$

$$T=\frac{(T^*-T_w)}{Sd^2/k}, \qquad Ra=\frac{\beta gSKd^3}{\alpha\nu k}\equiv\text{Rayleigh number} \tag{2}$$

and the dimensionless Darcy velocities are obtained from the stream function distribution according to the definitions

$$u=\frac{\partial\psi}{\partial y}, \qquad v=-\frac{\partial\psi}{\partial x}. \tag{3a, b}$$

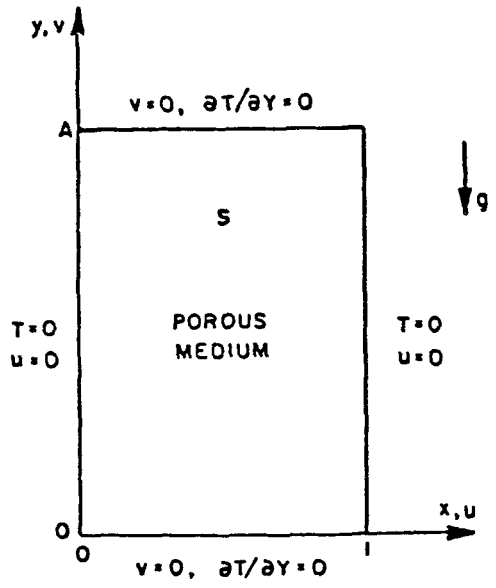

Figure 1. Geometry and co-ordinate system

Problem (1) above has a symmetry line at $x=1/2$, with a stagnation streamline dividing the flow into two identical cells. Therefore, alternative boundary conditions at this centreline are written as

$$\psi(1/2, y)=0, \qquad \frac{\partial T(1/2, y)}{\partial x}=0, \tag{4a, b}$$

which substitute equations (1d) and (1f) and the solution domain is redefined as $0\leqslant x\leqslant 1/2$, $0\leqslant y\leqslant A$.

The generalized integral transform technique[5,7-12] is now utilized to solve problem (1) and following the formalism in this approach, the appropriate auxiliary problems are chosen as

$$\frac{d^2\chi_i(x)}{dx^2}+\mu_i^2\chi_i(x)=0, \quad 0<x<\tfrac{1}{2}, \tag{5a}$$

$$\chi_i(0)=\chi_i\left(\frac{1}{2}\right)=0, \quad i=1, 2, \ldots \tag{5b, c}$$

for transformation of equation (1a) and

$$\frac{d^2\Gamma_n(x)}{dx^2}+\lambda_n^2\Gamma_n(x)=0, \quad 0<x<\tfrac{1}{2}, \tag{6a}$$

$$\Gamma_n(0)=0, \quad \frac{d\Gamma_n(1/2)}{dx}=0, \quad n=1, 2, \ldots \tag{6b, c}$$

for the transformation of equation (1b), where μ_i^2 and λ_n^2 are the respective eigenvalues, and $\chi_i(x)$ and $\Gamma_n(x)$ the associated normalized eigenfunctions, which are readily obtained in explicit form as

$$\chi_i(x)=2\sin\mu_i x; \quad \mu_i=2i\pi \tag{7a, b}$$

and

$$\Gamma_n(x)=2\sin\lambda_n x,\quad \lambda_n=(2n-1)\pi. \tag{7c, d}$$

The eigenvalue problems (5) and (6) are of the Sturm–Liouville type and allow definition of the following integral transform pairs:

$$\bar{\psi}_i(y)=\int_0^{1/2}\chi_i(x)\psi(x,y)\,dx,\quad \text{transform,} \tag{8a}$$

$$\psi(x,y)=\sum_{i=1}^{\infty}\chi_i(x)\bar{\psi}_i(y),\quad \text{inversion,} \tag{8b}$$

$$\bar{T}_n(y)=\int_0^{1/2}\Gamma_n(x)T(x,y)\,dx,\quad \text{transform,} \tag{8c}$$

$$T(x,y)=\sum_{n=1}^{\infty}\Gamma_n(x)\bar{T}_n(y),\quad \text{inversion.} \tag{8d}$$

We now operate on equation (1a) with $\int_0^{1/2}\chi_i(x)\,dx$, and make use of the boundary conditions (1c) and (4a), to obtain

$$\frac{d^2\bar{\psi}_i}{dy^2}-\mu_i^2\bar{\psi}_i(y)=-Ra\int_0^{1/2}\chi_i(x)\frac{\partial T(x,y)}{\partial x}\,dx. \tag{9a}$$

Similarly, equation (1b) is operated on with $\int_0^{1/2}\Gamma_n(x)\,dx$ and boundary conditions (1e) and (4b) are utilized, to yield

$$\frac{d^2\bar{T}_n}{dy^2}-\lambda_n^2\bar{T}_n(y)+\bar{f}_n=\int_0^{1/2}\Gamma_n(x)\frac{\partial\psi}{\partial y}\frac{\partial T}{\partial x}\,dx-\int_0^{1/2}\Gamma_n(x)\frac{\partial\psi}{\partial x}\frac{\partial T}{\partial y}\,dx, \tag{9b}$$

where the transformed heat generation term becomes

$$\bar{f}_n=\int_0^{1/2}\Gamma_n(x)\,dx\equiv\frac{2}{\lambda_n}. \tag{9c}$$

The non-transformable terms in equations (9a) and (9b) are now evaluated by substituting the inversion formulae (8b) and (8d) in the appropriate integrals, to provide

$$\int_0^{1/2}\chi_i(x)\frac{\partial T}{\partial x}\,dx=\sum_{j=1}^{\infty}a_{ij}\bar{T}_j(y), \tag{10a}$$

where

$$a_{ij}=\int_0^{1/2}\chi_i(x)\Gamma_j'(x)\,dx \tag{10b}$$

and prime denotes differentiation with respect to x. Also,

$$\int_0^{1/2}\Gamma_n(x)\frac{\partial\psi}{\partial y}\frac{\partial T}{\partial x}\,dx=\sum_{j=1}^{\infty}\sum_{k=1}^{\infty}B_{njk}\bar{T}_k(y)\frac{d\bar{\psi}_j}{dy}, \tag{10c}$$

where

$$B_{njk}=\int_0^{1/2}\Gamma_n(x)\chi_j(x)\Gamma_k'(x)\,dx \tag{10d}$$

and finally,

$$\int_0^{1/2} \Gamma_n(x) \frac{\partial \psi}{\partial x} \frac{\partial T}{\partial y} \, dx = \sum_{j=1}^{\infty} \sum_{k=1}^{\infty} B^*_{njk} \bar{\psi}_k(y) \frac{d\bar{T}_j}{dy}, \tag{10e}$$

where

$$B^*_{njk} = \int_0^{1/2} \Gamma_n(x) \Gamma_j(x) \chi'_k(x) \, dx. \tag{10f}$$

The integrals in equations (10b), (10d) and (10f) are readily integrated and obtained in analytical closed form. Equations (9a) and (9b) are then rewritten as

$$\frac{d^2\bar{\psi}_i}{dy^2} = \mu_i^2 \bar{\psi}_i(y) - Ra \sum_{j=1}^{\infty} a_{ij} \bar{T}_j(y), \quad i = 1, 2, \ldots, \infty, \tag{11a}$$

$$\frac{d^2\bar{T}_n}{dy^2} = \lambda_n^2 \bar{T}_n(y) + \sum_{j=1}^{\infty} \sum_{k=1}^{\infty} \left[B_{njk} \bar{T}_k \frac{d\bar{\psi}_j}{dy} - B^*_{njk} \bar{\psi}_k \frac{d\bar{T}_j}{dy} \right] - \bar{f}_n, \quad n = 1, 2, \ldots \tag{11b}$$

The corresponding boundary conditions are obtained through the appropriate integral transformation of equations (1g)–(1j), that results in

$$\bar{\psi}_i(0) = 0, \qquad \bar{\psi}_i(A) = 0, \tag{11c, d}$$

$$\frac{d\bar{T}_n(0)}{dy} = 0, \qquad \frac{d\bar{T}_n(A)}{dy} = 0. \tag{11e, f}$$

System (11) above forms an infinite set of coupled second-order non-linear ODEs subjected to boundary conditions at two points. For computational purposes, the system is truncated at a sufficiently large finite order for the desired precision, which corresponds to truncating the expansions for ψ at the Nth term and the expansions for T at the Mth term. The formal aspects that warrant convergence of the truncated system to the infinite system solution, as $N, M \to \infty$, are discussed in Reference 5 and are not repeated here. The truncated system then becomes, in normal form

$$\mathbf{w}' = \mathbf{p}(\mathbf{w}, y) \tag{12a}$$

where the solution vector $\mathbf{w}$ is given by

$$\mathbf{w} = \left\{ \bar{\psi}_1, \ldots, \bar{\psi}_N, \frac{d\bar{\psi}_1}{dy}, \ldots, \frac{d\bar{\psi}_N}{dy}, \bar{T}_1, \ldots, \bar{T}_M, \frac{d\bar{T}_1}{dy}, \ldots, \frac{d\bar{T}_M}{dy} \right\}^{\mathrm{T}} \tag{12b}$$

and

$$\mathbf{p}(\mathbf{w}, y) = \begin{cases} w_{N+l}, \quad 1 \leqslant l \leqslant N, & (12c) \\ \mu^2_{l-N} w_{l-N} - Ra \sum_{j=1}^{M} a_{l-N,j} w_{2N+j}, \quad (N+1) \leqslant l \leqslant 2N, & (12d) \\ w_{M+l}, \quad (2N+1) \leqslant l \leqslant (2N+M), & (12e) \\ \lambda^2_{l-(2N+M)} w_{l-M} + \sum_{j=1}^{N} \sum_{k=1}^{M} B_{l-(2N+M),j,k} w_{2N+k} w_{N+j} \\ \quad - \sum_{j=1}^{M} \sum_{k=1}^{N} B^*_{l-(2N+M),j,k} w_{2N+M+j} - \bar{f}_{l-(2N+M)}, \\ \quad (2N+M+1) \leqslant l \leqslant (2N+2M), & (12f) \end{cases}$$

with boundary conditions

$$w_l(0)=0, \qquad w_l(A)=0, \qquad 1\leqslant l\leqslant N, \tag{12g, h}$$

$$w_{2N+M+l}(0)=0, \qquad w_{2N+M+l}(A)=0, \qquad 1\leqslant l\leqslant M. \tag{12i, j}$$

The boundary value problem (12) is in a suitable form for the application of well-established algorithms available in scientific subroutine packages, such as the IMSL library.[14] Subroutine DBVPFD in this library is one example of a reliable boundary value problem solver, which allows for automatic error control, until the required accuracy is achieved. Once the transformed potentials $\bar{\psi}_i$ and $\bar{T}_n$, have been obtained with prescribed precision, the inversion formulae, equations (8b) and (8d), are recalled to provide an explicit analytic expression for the original potentials, $\psi(x, y)$ and $T(x, y)$, at any desired position.

RESULTS AND DISCUSSION

The present problem was solved for different values of the governing parameters, Rayleigh number and aspect ratio, namely, $A=0{\cdot}1, 0{\cdot}2, 0{\cdot}5, 1{\cdot}0, 2{\cdot}0, 5{\cdot}0$ and $10{\cdot}0$, $Ra=10, 50, 100, 500$ and 1000.

First, the convergence behaviour of this eigenfunction expansion-type approach is illustrated in Tables I and II, for stream function and temperature, respectively, with $Ra=100$ and $A=5$. To

Table I. Convergence of temperature distribution ($N=M$, tolerance $=10^{-4}$, $Ra=100$; $A=5$)

y	N	$x=0{\cdot}1$	$x=0{\cdot}2$	$x=0{\cdot}3$	$x=0{\cdot}4$	$x=0{\cdot}5$
	5	0·03210	0·05924	0·08182	0·09713	0·1028
	9	0·03200	0·05931	0·08179	0·09719	0·1028
0·0	13	0·03202	0·05932	0·08178	0·09718	0·1027
	17	0·03202	0·05932	0·08178	0·09718	0·1027
	22	0·03202	0·05932	0·08179	0·09719	0·1027
	5	0·03390	0·06136	0·08355	0·09820	0·1036
	9	0·03378	0·06145	0·08350	0·09828	0·1035
0·1111	13	0·03379	0·06146	0·08350	0·09827	0·1035
	17	0·03380	0·06145	0·08350	0·09827	0·1035
	22	0·03379	0·06145	0·08350	0·09827	0·1035
	5	0·04493	0·07953	0·1046	0·1193	0·1244
	9	0·04479	0·07962	0·1045	0·1194	0·1244
2·2222	13	0·04480	0·07963	0·1045	0·1194	0·1244
	17	0·04481	0·07963	0·1045	0·1194	0·1244
	22	0·04480	0·07963	0·1045	0·1194	0·1244
	5	0·06142	0·1025	0·1271	0·1397	0·1438
	9	0·06124	0·1026	0·1270	0·1398	0·1437
4·8889	13	0·06126	0·1026	0·1270	0·1397	0·1437
	17	0·06126	0·1026	0·1270	0·1397	0·1437
	22	0·06126	0·1026	0·1270	0·1397	0·1437
	5	0·06583	0·1063	0·1299	0·1415	0·1454
	9	0·06553	0·1065	0·1297	0·1416	0·1453
5·0000	13	0·06556	0·1065	0·1297	0·1416	0·1453
	17	0·06556	0·1065	0·1297	0·1416	0·1453
	22	0·06556	0·1065	0·1297	0·1416	0·1453

simplify the tables, the truncation orders in the two expansions were kept equal, i.e. $N=M$, and varying from $M=5$ up to 22. The ODE solver was employed with a required tolerance of 10^{-4}, which means that the fully converged results are expected to be correct to ± 1 in the fourth significant digit. The tables present results for ψ and T at various locations within the cavity, in order to cover all the regions of different physical and mathematical behaviour. From an inspection of Table I, it can be noticed that the temperature results for $N=9$ are, in general, already fully converged to the four digits required, with a slightly slower convergence rate close to the wall at $x=0$, within the boundary layer. From Table II, the stream function results demonstrate to be essentially fully converged for $N=13$, again with some slight improvement in convergence for the more internal points in the horizontal direction. Similar conclusions concerning this well-behaved convergence were drawn for the other cases tested, with almost uniform convergence rates within the medium.

Figures 2–4 show comparisons of the present integral transform solutions with the finite difference results in Reference 1, for all the three dependent variables, horizontal velocity, vertical velocity and temperature, with different values of Ra and A. The fully converged integral transform results obtained within prescribed accuracy, validate the discrete approach results in all situations considered, both in the interior of the enclosure and in the vicinity of the top and bottom end walls, where all three variables experience more significant variations. These results were obtained with $N=M\leqslant 18$, and a relative error target for the boundary value problem solver of 10^{-4}. A typical run in the VAX 8810 computer takes about 138 s of CPU time.

Table II. Convergence of stream function distribution ($N=M$, tolerance $=10^{-4}$, $Ra=100$, $A=5$)

y	N	$x=0{\cdot}1$	$x=0{\cdot}2$	$x=0{\cdot}3$	$x=0{\cdot}4$	$x=0{\cdot}5$
	5	0·2790	0·3424	0·2969	0·1673	0·0
	9	0·2736	0·3446	0·2951	0·1678	0·0
0·1111	13	0·2744	0·3451	0·2952	0·1681	0·0
	17	0·2743	0·3451	0·2953	0·1679	0·0
	22	0·2743	0·3450	0·2953	0·1679	0·0
	5	0·5823	0·7634	0·6719	0·3814	0·0
	9	0·5752	0·7660	0·6693	0·3821	0·0
1·1111	13	0·5763	0·7666	0·6694	0·3824	0·0
	17	0·5762	0·7666	0·6696	0·3822	0·0
	22	0·5761	0·7666	0·6696	0·3822	0·0
	5	0·6030	0·7921	0·6981	0·3967	0·0
	9	0·5957	0·7948	0·6955	0·3974	0·0
2·2222	13	0·5969	0·7954	0·6956	0·3976	0·0
	17	0·5967	0·7954	0·6957	0·3974	0·0
	22	0·5966	0·7954	0·6957	0·3975	0·0
	5	0·6060	0·7964	0·7019	0·3989	0·0
	9	0·5987	0·7991	0·6993	0·3996	0·0
3·3333	13	0·5999	0·7997	0·6994	0·3999	0·0
	17	0·5997	0·7997	0·6996	0·3997	0·0
	22	0·5997	0·7996	0·6996	0·3997	0·0
	5	0·6177	0·8019	0·6995	0·3944	0·0
	9	0·6101	0·8048	0·6967	0·3952	0·0
4·4444	13	0·6113	0·8054	0·6968	0·3955	0·0
	17	0·6111	0·8054	0·6970	0·3952	0·0
	22	0·6111	0·8053	0·6970	0·3952	0·0

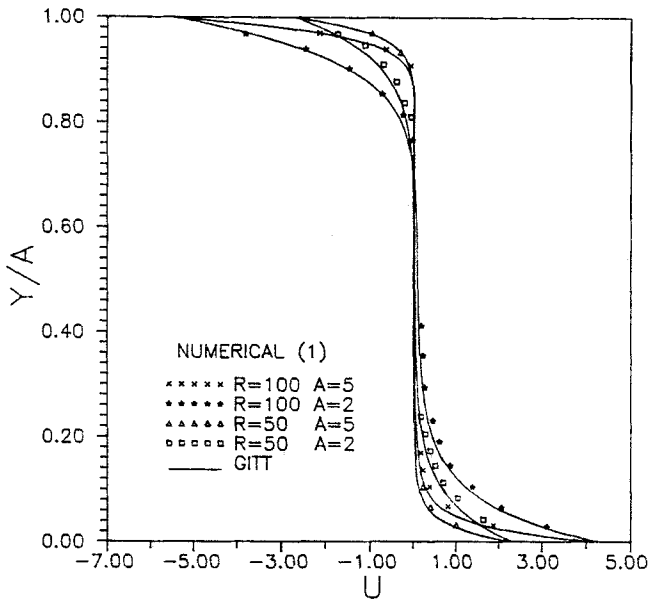

Figure 2. Comparison of generalized integral transform solution (GITT) with finite differences results:[1] horizontal velocity profiles along $x=0{\cdot}2$

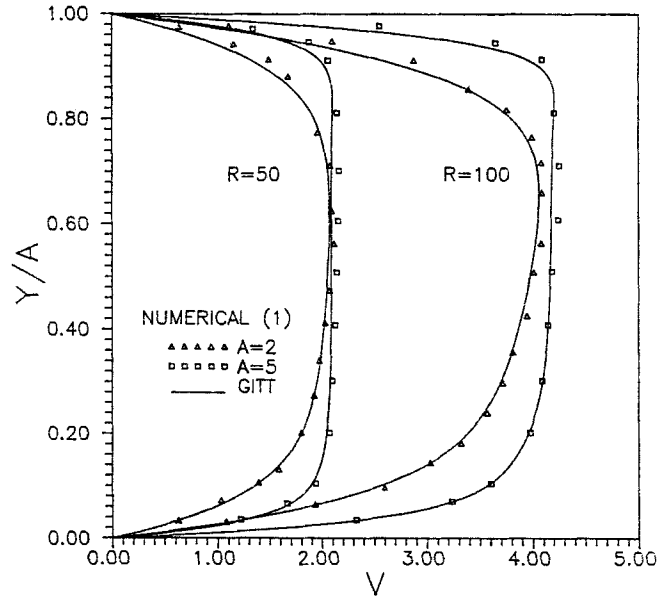

Figure 3. Comparison of generalized integral transform solution (GITT) with finite differences results:[1] vertical velocity profiles along the vertical centreline ($x=0{\cdot}5$)

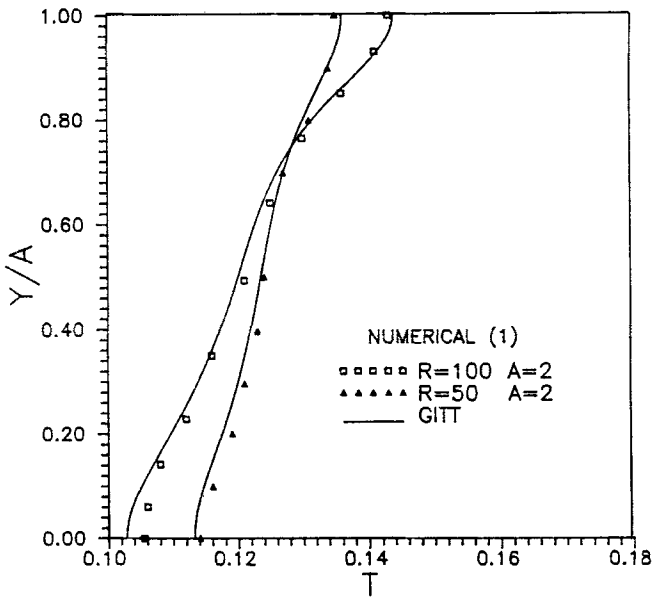

Figure 4. Comparison of generalized integral transform solution with finite differences results:[1] temperature profiles along the centreline ($x = 0{\cdot}5$)

Table III brings the influence of aspect ratio on the convergence rates of both temperature and stream function distributions, for the case of $Ra = 100$, relative error target of 10^{-4} and $A = 10$, 1, or 0·2. Only the higher values of the truncation order, N, are presented, in order to make the analysis of convergence more clear. For the temperature distribution, the convergence characteristics are essentially independent of the aspect ratio, either large or small, for representative positions within the medium, including the vicinity of the walls. The stream function distributions, although presenting slower convergence rates when compared to the temperature behaviour, again do not seem to be markedly affected by the value of A. With similar concerns, Table IV illustrates the influence of Rayleigh number on convergence rates of temperature and stream function distributions, for the case of $A = 1$ and taking the values $Ra = 50$ and 500. Clearly, in the range of parameters considered, the increase in Ra does not significantly affect the convergence behaviour, with some slight slowing down for the convergence at $x = 0{\cdot}05$. For very high Rayleigh number, however, the source term in the stream function problem might increase markedly and cause much slower convergence. In such situations, filtering procedures, alternative enhanced series and/or coupled auxiliary problems[5,15] may be employed to overcome such difficulties, in case the consideration of larger truncation orders is to be avoided.

Table V demonstrates the influence of the relative error target requested to the boundary value problem solver, on the final results for both temperature and stream function, illustrated here for the case $Ra = 100$, $A = 2$, and taking a truncation order of $N = 10$. Representative values for the input tolerances were considered, tolerance $= 10^{-4}$, 10^{-5}, 10^{-6} and 10^{-7}, and even lower values could have been adopted. However, it is clear from this table, that the error control scheme in this subroutine is a conservative one, and it more than suffices to fix the ODE solver tolerance to the number of correct digits desired in the final solutions. The value of tolerance $= 10^{-4}$ provides even six correct digits in most cases considered.

Table III. Influence of aspect ratio (A) on convergence of temperature and stream function distributions ($Ra=100$, tolerance $=10^{-4}$)

		$T(x, y)$					
		$A=10$		$A=1$		$A=0{\cdot}2$	
y	N	$x=0{\cdot}1$	$x=0{\cdot}5$	$x=0{\cdot}1$	$x=0{\cdot}5$	$x=0{\cdot}1$	$x=0{\cdot}5$
0·0	10	0·03200	0·1027	0·03234	0·1043	0·04217	0·1240
	12	0·03201	0·1027	0·03235	0·1043	0·04218	0·1240
	14	0·03202	0·1027	0·03236	0·1043	0·04219	0·1240
	16	0·03202	0·1027	0·03236	0·1043	0·04219	0·1240
	18	0·03202	0·1027	0·03236	0·1043	0·04219	0·1240
A	10	0·06553	0·1453	0·06075	0·1362	0·04751	0·1245
	12	0·06555	0·1453	0·06077	0·1363	0·04753	0·1245
	14	0·06557	0·1453	0·06079	0·1363	0·04754	0·1245
	16	0·06557	0·1453	0·06079	0·1363	0·04754	0·1245
	18	0·06556	0·1453	0·06078	0·1363	0·04754	0·1245
		$\psi(x, y)$					
y	N	$x=0{\cdot}1$	$x=0{\cdot}4$	$x=0{\cdot}1$	$x=0{\cdot}4$	$x=0{\cdot}1$	$x=0{\cdot}4$
2·222 ($A=10$)	10	0·5957	0·3974	0·4078	0·2608	0·0315	0·0105
	12	0·5965	0·3973	0·4089	0·2609	0·0320	0·0105
0·222 ($A=1$)	14	0·5970	0·3975	0·4084	0·2608	0·0322	0·0106
	16	0·5969	0·3976	0·4087	0·2610	0·0322	0·0106
0·011 ($A=0{\cdot}2$)	18	0·5966	0·3976	0·4085	0·2610	0·0320	0·0106
8·889 ($A=10$)	10	0·6012	0·4012	0·3634	0·1682	0·0760	0·0244
	12	0·6020	0·4011	0·3651	0·1683	0·0768	0·0243
0·889 ($A=1$)	14	0·6025	0·4013	0·3644	0·1681	0·0773	0·0245
	16	0·6024	0·4014	0·3649	0·1685	0·0772	0·0246
0·170 ($A=0{\cdot}2$)	18	0·6021	0·4014	0·3645	0·1685	0·0769	0·0246

Figure 5 shows a comparison of local Nusselt number along the vertical wall ($x=0$), obtained from the expression

$$Nu=2\,\frac{\partial T(0, y)}{\partial x}. \tag{13}$$

For a best computational performance, the derivative in equation (13) above is not evaluated directly from the analytical differentiation of the inverse formula, equation (8d), since this approach produces a slower converging series due to the appearance of the monotonically increasing eigenvalue in the derivative expression. This well-known behaviour in eigenfunction expansions is easily avoided by considering instead, the alternative enhanced series produced by the integral energy balance,[5,15] i.e. through integration of the energy equation, equation (1b), within the x domain, to yield

$$\left.\frac{\partial T}{\partial x}\right|_{x=0}=\frac{1}{2}+\frac{d^2}{dy^2}\left(\int_0^{1/2} T(x, y)\,dx\right)+\int_0^{1/2}\left(\frac{\partial \psi}{\partial y}\frac{\partial T}{\partial x}-\frac{\partial \psi}{\partial x}\frac{\partial T}{\partial y}\right)dx, \tag{14}$$

Table IV. Influence of Rayleigh number (Ra) on convergence of temperature and stream function distributions ($A=1$, tolerance $=10^{-4}$)

		$T(x, y)$			
		$Ra=50$		$Ra=500$	
y	N	$x=0{\cdot}05$	$x=0{\cdot}25$	$x=0{\cdot}05$	$x=0{\cdot}25$
0	16	0·01982	0·08222	0·00887	0·03895
	18	0·01981	0·08222	0·00887	0·03895
	20	0·01981	0·08222	0·00887	0·03895
	22	0·01981	0·08222	0·00887	0·03895
1·0	16	0·02846	0·1044	0·05503	0·1102
	18	0·02845	0·1044	0·05499	0·1102
	20	0·02845	0·1044	0·05498	0·1102
	22	0·02845	0·1044	0·05499	0·1102
		$\psi(x, y)$			
y	N	$x=0{\cdot}05$	$x=0{\cdot}2$	$x=0{\cdot}05$	$x=0{\cdot}2$
0·222	16	0·1343	0·2851	0·7909	1·685
	18	0·1342	0·2851	0·7903	1·685
	20	0·1342	0·2851	0·7902	1·684
	22	0·1342	0·2852	0·7903	1·685
0·889	16	0·1149	0·2073	1·125	1·359
	18	0·1148	0·2072	1·123	1·359
	20	0·1148	0·2073	1·123	1·358
	22	0·1148	0·2073	1·123	1·359

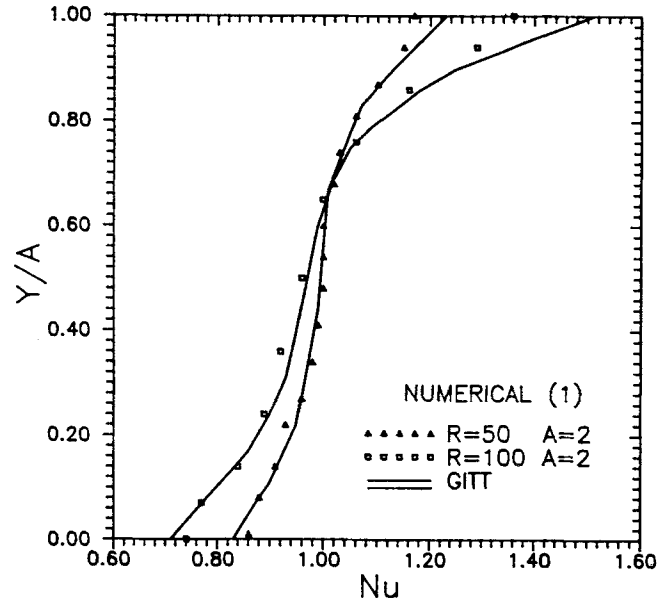

Figure 5. Comparison of Nusselt number along cooled wall, at $x=0$, with finite differences results[1]

which is readily evaluated in analytic form upon substitution of the inversion formulae in the integrals above.

Here some deviations are observed between the two solution procedures, specially in the vicinity of the top end wall and for increasing Rayleigh number. The integral transform results for

Table V. Influence of local relative error for the ODE solver[12] on the global error of temperature and stream function ($N=10$, $Ra=100$, $A=2$)

y	Tolerance	$x=0{\cdot}1$	$x=0{\cdot}2$	$T(x, y)$ $x=0{\cdot}3$	$x=0{\cdot}4$	$x=0{\cdot}5$
0·0	10^{-4}	0·0319997	0·0593035	0·0817784	0·0971804	0·1027412
	10^{-5}	0·0319996	0·0593034	0·0817784	0·0971803	0·1027411
	10^{-6}	0·0319996	0·0593034	0·0817784	0·0971803	0·1027411
	10^{-7}	0·0319996	0·0593034	0·0817784	0·0971803	0·1027411
2·0	10^{-4}	0·0647013	0·1051842	0·1282621	0·1400795	0·1437189
	10^{-5}	0·0647013	0·1051843	0·1282622	0·1400796	0·1437190
	10^{-6}	0·0647013	0·1051843	0·1282622	0·1400796	0·1437190
	10^{-7}	0·0647013	0·1051843	0·1282622	0·1400796	0·1437190
				$\psi(x, y)$		
0·111	10^{-4}	0·2736110	0·3446482	0·2951457	0·1678918	0·0
	10^{-5}	0·2736110	0·3446480	0·2951455	0·1678917	0·0
	10^{-6}	0·2736110	0·3446480	0·2951455	0·1678917	0·0
	10^{-7}	0·2736110	0·3446480	0·2951455	0·1678917	0·0
1·903	10^{-4}	0·3584616	0·3961861	0·3047445	0·1616959	0·0
	10^{-5}	0·3584617	0·3961862	0·3047446	0·1616959	0·0
	10^{-6}	0·3584617	0·3961862	0·3047446	0·1616959	0·0
	10^{-7}	0·3584617	0·3961862	0·3047446	0·1616959	0·0

Table VI. Convergence of Nusselt number and the relative error in the overall energy balance

N	$y=0{\cdot}0$	$y=0{\cdot}5$	$y=1{\cdot}0$	Error (%) (energy balance)
		($Ra=50$, $A=2$, tolerance $=10^{-4}$)		
10	0·8288	0·9913	1·232	0·00106
13	0·8287	0·9913	1·232	0·00258
15	0·8286	0·9913	1·232	0·00234
17	0·8286	0·9913	1·232	0·00182
19	0·8286	0·9913	1·232	0·00016
21	0·8285	0·9913	1·232	0·00053
		($Ra=100$, $A=2$, tolerance $=10^{-4}$)		
N	$y=0{\cdot}0$	$y=0{\cdot}5$	$y=1{\cdot}0$	Error (%) (energy balance)
10	0·7094	0·9811	1·508	0·00819
13	0·7092	0·9811	1·510	0·00671
15	0·7091	0·9811	1·510	0·00594
17	0·7090	0·9811	1·510	0·00564
19	0·7090	0·9811	1·510	0·00576
21	0·7090	0·9811	1·511	0·00473

Nusselt number are, however, fully converged to four significant digits with $N=M\leqslant 20$, as illustrated in Table VI for these two cases ($Ra=50$, $A=2$ and $Ra=100$, $A=2$). Therefore, deviations on the Nusselt number results are most probably due to the propagation of errors in the numerical differentiation of the discrete information from the finite differences solution. In order to confirm this observation, we have computed the relative error in the overall energy balance, which is also presented in Table VI. While the finite differences solution in Reference 1 achieved an order of 2% relative error in the energy balance, the present results reach errors of only 0·0001%, as good as it could be, in accordance with the requested accuracy.

Figures 6(a) and 6(b) present one set of streamlines and isotherms, respectively, in the case of $Ra=500$ and $A=2$, for reference purposes. All the physical trends pointed out in Reference 1 are observed here. Near the cold walls, the convective motion becomes more important and isotherms are more closely spaced. The point of maximum ψ is closer to the top and the flow pattern is asymmetric in the vertical direction. Isotherms are flatter at the top of the enclosure and more parallel at the bottom where conduction predominates.

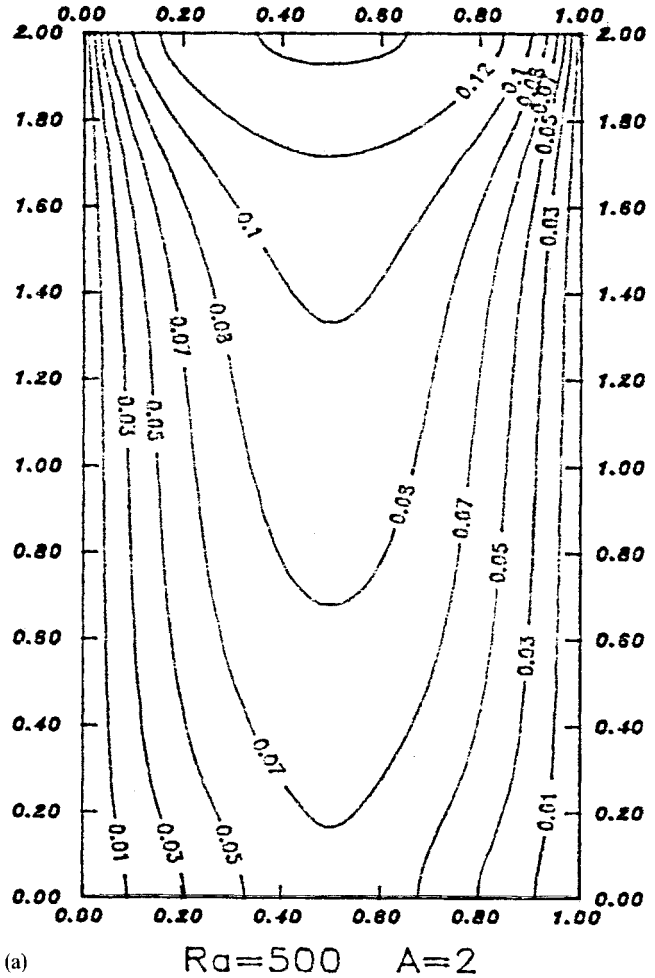

Figure 6. (a) Streamlines for $Ra=500$ and $A=2$ (b) Isotherms for $Ra=500$ and $A=2$

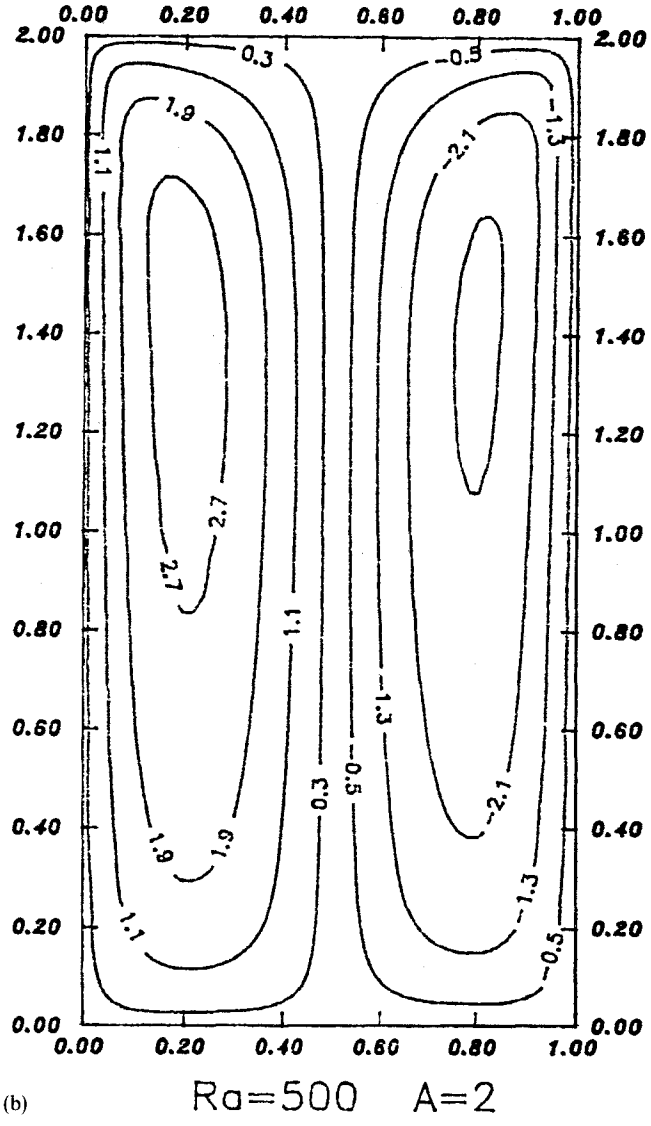

Figure 6. (Continued)

Finally, it should be noted that this approach under development is already flexible enough to be extended to more complex problems, such as in the cases of multilayered media, irregular geometries, moving boundaries, variable properties, etc., by combining different and recent contributions in the generalized integral transform technique.[5] The analysis of transient problems shall also follow, through application of successive integral transformations in each spatial co-ordinate, as discussed in Reference 5, and numerically solving the resulting initial value problem with automatic control of the relative error. In addition, more general models than the Darcian flow analysed here, may be considered, including non-linear convective terms in the momentum equations, such as in the case of the full Navier–Stokes equations,[11,12] recently handled through the same approach.

APPENDIX: NOMENCLATURE

A	aspect ratio ($=h/d$)
d	width of enclosure
g	acceleration due to gravity
h	height of enclosure
k	effective thermal conductivity
K	permeability
M, N	number of terms in truncated expansions
Ra	Rayleigh number ($=\beta g S K d^3/\alpha \nu k$)
S	uniform volumetric heat generation rate
T, T^*	temperature distribution, dimensionless and dimensional
T_w	cold walls temperature
u, v	horizontal and vertical velocities, dimensionless
x, x^*	horizontal co-ordinate, dimensionless and dimensional
y, y^*	vertical co-ordinate, dimensionless and dimensional
α	effective thermal diffusivity
β	coefficient of volumetric expansion
λ_n	eigenvalues of problem (6)
μ_i	eigenvalues of problem (5)
ν	kinematic viscosity
ψ, ψ^*	stream function, dimensionless and dimensional
——	integral transformed quantity
i, n	order of eigenvalue

REFERENCES

1. M. Haajizadeh, A. F. Ozguc and C. L. Tien, 'Natural convection in a vertical porous enclosure with internal heat generation', *Int. J. Heat Mass Transfer*, **27,** 1893–1902 (1984).
2. V. Prasad and F. A. Kulacki, 'Natural convection in a rectangular porous cavity with constant heat flux on one vertical wall', *J. Heat Transfer*, **106,** 152–157 1(984).
3. F. C. Lai and F. A. Kulacki, 'Natural convection across a vertical layered porous cavity', *Int. J. Heat Mass Transfer*, **31,** 1247–1260 (1988).
4. R. Rajamani, C. Srinivas and K. N. Seetharamu, 'Finite element analysis of convective heat transfer in porous media', *Int. j. numer. methods fluids*, **11,** 331–339 (1990).
5. R. M. Cotta, *Integral Transforms in Computational Heat and Fluid Flow*, CRC Press, Boca Raton, FL, 1992.
6. M. D. Mikhailov and M. N. Özisik, *Unified Analysis and Solutions of Heat and Mass Diffusion*, Wiley, New York, 1984.
7. R. M. Cotta, 'Hybrid numerical–analytical approach to nonlinear diffusion problems', *Numer. Heat Transfer* (Part B), **17,** 217–226 (1990).
8. R. Serfaty and R. M. Cotta, 'Integral transform solutions of diffusion problems with non-linear equation coefficients', *Int. Commun. Heat Mass Transfer*, **17,** 851–864 (1990).
9. R. Serfaty and R. M. Cotta, 'Hybrid analysis of transient nonlinear convection–diffusion problems', *Int. J. Numer. Meth. Heat Fluid Flow*, **2,** 55–62 (1992).
10. R. M. Cotta and T. M. B. Carvalho, 'Hybrid analysis of boundary layer equations for internal flow problems', *Proc. 7th Int. Conf. Numer. Methods Laminar and Turbulent Flow (Part 1)*, Stanford, CA, 1991, pp. 106–115.
11. J. S. Perez Guerrero and R. M. Cotta, 'Integral transform method for Navier–Stokes equations in streamfunction-only formulation', *Int. j. numer. methods fluids*, **15,** 399–409 (1992).
12. R. M. Cotta, J. S. Perez Guerrero and F. Scofano Neto, 'Hybrid solution of the incompressible Navier–Stokes equations via integral transformation', *Proc. II Int. Conf. on Adv. Comp. Methods in Heat Transfer, Heat Transfer 92*, Vol. 1, Milan, Italy, 1992, pp. 735–750.
13. S. V. Patankar, *Numerical Heat Transfer and Fluid Flow*, McGraw-Hill, New York, 1980.
14. *IMSL Library*, MATH/LIB, Houston, TX, 1987.
15. F. Scofano Neto, R. M. Cotta and M. D. Mikhailov, 'Alternative approach to the integral transform solution of nonhomogeneous diffusion problems', *Proc. Int. Conf. on Advanced Comp. Methods in Heat Transfer*, Vol. 1, Southampton, UK, 1990, pp. 39–50.